High-harmonic fast wave heating and current drive results for deuterium H-mode plasmas in the National Spherical Torus Experiment

G. Taylor[1], P.T. Bonoli[2], R.W. Harvey[3], J.C. Hosea[1], E.F. Jaeger[4], B.P. LeBlanc[1], C.K. Phillips[1], P.M. Ryan[4], E.J. Valeo[1], J.R. Wilson[1], J.C. Wright[2], and the NSTX Team

[1]*Princeton Plasma Physics Laboratory, Princeton, NJ, USA*

[2]*Plasma Science and Fusion Center, MIT, Cambridge, MA, USA*

[3]*CompX, Del Mar, CA, USA*

[4]*Oak Ridge National Laboratory, Oak Ridge, TN, USA*

A critical research goal for the spherical torus (ST) program is to initiate, ramp-up, and sustain a discharge without using the central solenoid. Simulations of non-solenoidal plasma scenarios in the National Spherical Torus Experiment (NSTX) [1] predict that high-harmonic fast wave (HHFW) heating and current drive (CD) [2] can play an important roll in enabling fully non-inductive ($f_{NI} \sim 1$) ST operation. The NSTX $f_{NI} \sim 1$ strategy requires 5-6 MW of HHFW power (P_{RF}) to be coupled into a non-inductively generated discharge [3] with a plasma current, $I_p \sim 250$-350 kA, driving the plasma into an HHFW H-mode with $I_p \sim 500$ kA, a level where 90 keV deuterium neutral beam injection (NBI) can heat the plasma and provide CD. The initial approach on NSTX has been to heat $I_p \sim 300$ kA, inductively heated, deuterium plasmas with CD phased HHFW power [2], in order to drive the plasma into an H-mode with $f_{NI} \sim 1$. As a result of better plasma conditioning and reduced plasma control system latency, recent experiments have achieved $f_{NI} \sim 0.65$ with $P_{RF} = 1.4$ MW in a $I_p = 300$ kA plasma, using a launched toroidal mode number, $k_\phi = -8$ m^{-1} (CD phasing). Figure 1(a) shows Thomson scattering electron density profiles ($n_e(R)$) and electron temperature profiles ($T_e(R)$) for this plasma (shot 138506). $T_e(0)$ increased from 0.3 to 3 keV during the HHFW pulse, and $n_e(R)$ developed a steep edge pedestal characteristic of the H-mode, and eventually a hollow core inside an internal transport barrier (ITB). The total plasma stored energy (W_{tot}) increased from 5 kJ before HHFW heating (0.165 s) to 20 kJ near the end of the HHFW pulse (0.382 s). The RF

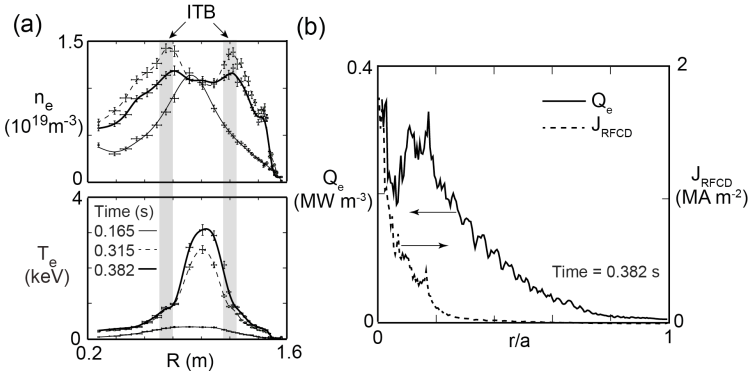

Fig. 1. (a) $n_e(R)$ and $T_e(R)$ before the start of HHFW heating (0.165s) and during HHFW heating (0.315 and 0.382 s), when an HHFW-generated H-mode and ITB had developed during an $I_p = 300$ kA, $B_T(0) = 5.5$ kG plasma (shot 138506). (b) RF electron power deposition (Q_e) and RF-driven current density (J_{RFCD}) profiles versus r/a, calculated by GENRAY-ADJ at 0.382 s, for 1 MW of coupled RF power.

electron power deposition (Q_e) profile and RF-driven current density (j_{RFCD}) profile were calculated by GENRAY-ADJ [4] at 0.382 s in shot 138506, for P_{RF} = 1 MW (Fig. 1(b)). Q_e and j_{RFCD} are peaked on axis. More than 95% of the RF power coupled inside the last closed flux surface (LCFS) directly heats electrons and the RF CD efficiency, ξ_{cd}, is ~ 0.1 MA/MW.

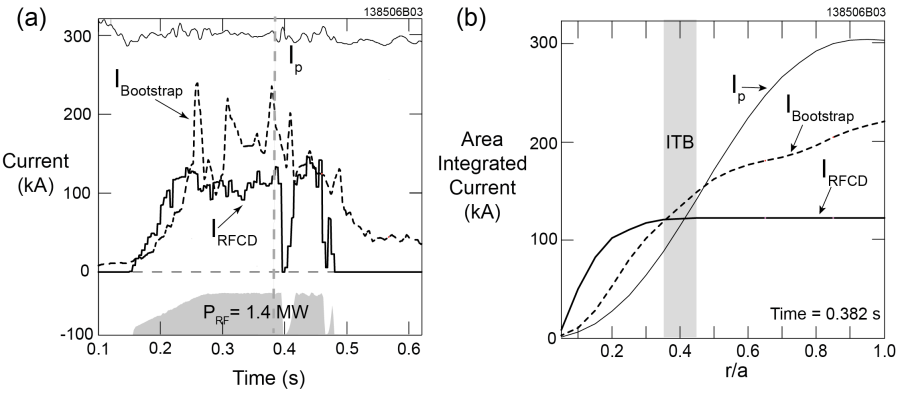

Fig. 2. TRANSP-TORIC full wave simulation results for shot 138506, assuming η_{eff} = 100%. (a) Time evolution of I_p (thin solid line), I_{RFCD} (thick solid line) and $I_{Bootstrap}$ (dashed line) and the RF power waveform (grey shading). (b) Area integrated current versus normalized minor radius at 0.382 s, the time indicated by the vertical dashed grey line in (a).

The time evolution of Q_e and j_{RFCD} for shot 138506 were modeled with a version of the TORIC full-wave code [5] integrated into the TRANSP transport code [6]. Results from this modeling, which assumes the RF coupling efficiency, η_{eff} = 100%, are shown in Fig. 2. The I_{RFCD} reaches 120 kA (Fig. 2(a)) and is entirely driven within the ITB (Fig. 2(b)). 60% of the bootstrap current ($I_{Bootstrap}$) is driven inside the ITB (Fig 2(b)). $I_{Bootstrap}$ fluctuates between 100 and 200 kA (Fig. 2(a)) as the pressure gradient at the ITB changes. These results predict f_{NI} ~ 1 if η_{eff} = 100%, however there are not insignificant RF coupling losses for this plasma. An estimate of the actual η_{eff} can be obtained from $\eta_{eff} = \Delta W_{tot}/(\tau * P_{RF})$, where the change in stored energy during RF heating, ΔW_{tot} ~ 15 kJ, P_{RF} = 1.4 MW, and the total energy confinement time, τ ~ 15 ms, yielding η_{eff} ~ 60%. Using this η_{eff}, $I_{Bootstrap}$ ~ 130 kA and I_{RFCD} ~ 70kA, so that f_{NI} ~ 0.65.

k_ϕ = -8 m^{-1} HHFW power was also coupled into an I_p = 300 kA, $B_T(0)$ = 5.5 kG NBI-generated H-mode, and the results are summarized in Fig. 3. Figure 3(a) compares the time evolution of $T_e(0)$ and n_eL for two similar I_p = 300 kA NBI H-mode discharges, one with P_{RF} = 1.4 MW and P_{NBI} = 2 MW (solid lines, shot 140352), and the other with only P_{NBI} = 2 MW (dashed lines, shot 140353). As P_{RF} is ramped up in shot 140352 there is initially a significant increase in $T_e(0)$ from 0.7 to 1.4 keV compared to shot 140353. However, n_eL begins to increase at the start of the HHFW pulse, so that at 0.450 s in shot 140352 $n_eL = 2.7 \times 10^{19}$ m^{-2}, compared to 1.4×10^{19} m^{-2} in shot 140353. At 0.450 s during shot 140352 the T_e profile is peaked on axis and the n_e profile has a steep edge density pedestal (Fig. 3(b)). At this time the RF deposition is peaked on axis (Fig. 3(c)), with 58% of the RF power directly heating electrons and 42% accelerating NBI fast ions. Most of the RF-accelerated fast-ions are poorly confined and promptly lost. The density rise for shot 140352, shown in

Fig. 3(a), is due to the increased interaction of fast-ions with the antenna caused by the RF-induced enhanced loss of fast-ions. ξ_{cd} is only ~ 0.02 MA/MW for shot 140352, significantly lower than for shot 138506, due to the higher $n_e(0)$, lower $T_e(0)$, and the RF power lost to fast-ion acceleration. Figure 3(d) shows the area integrated current versus r/a at 0.450 s calculated by TRANSP-TORIC for shot 140352 (solid lines) and 140353 (dashed lines), assuming η_{eff} = 100%. The actual η_{eff} for these shots was only ~ 40%, yielding f_{NI} ~ 0.45 for shot 140352 and f_{NI} ~ 0.4 for shot 140353.

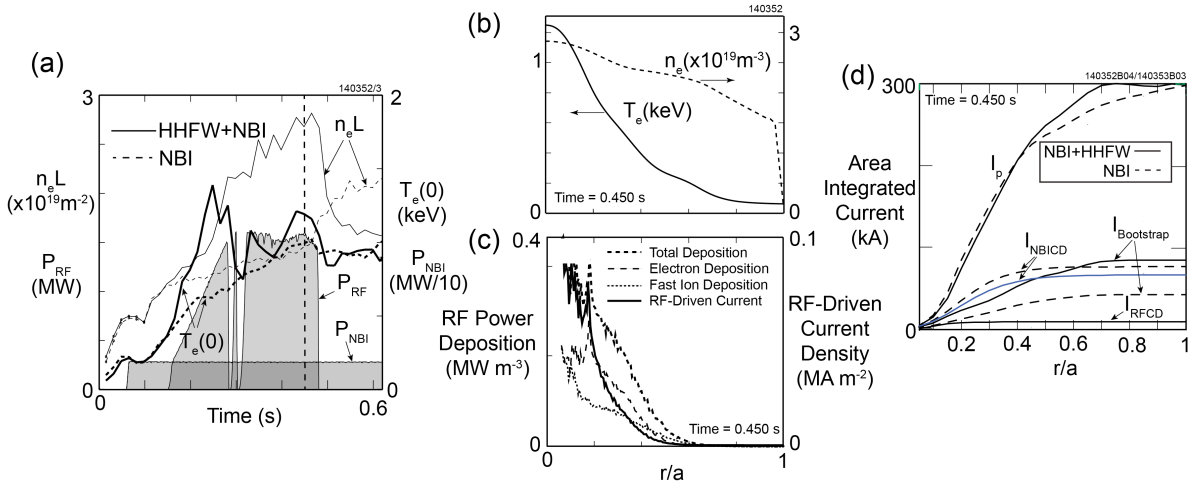

Fig. 3. (a) Time evolution of $T_e(0)$ and n_eL for two similar I_p = 300 kA NBI H-modes, one with P_{RF} = 1.4 MW and P_{NBI} = 2 MW (solid lines, shot 140352), and the other with only P_{NBI} = 2 MW (dashed lines, shot 140353). (b) $T_e(r/a)$ and $n_e(r/a)$, and (c) RF depostion and RF-driven current calculated by GENRAY-ADJ for P_{RF} = 1 MW, at 0.450 s during shot 140352. (d) Area integrated I_p, I_{NBICD}, $I_{Bootstrap}$, and I_{RFCD} versus r/a calculated at 0.450 s by TRANSP-TORIC, assuming η_{eff} = 100%.

Another role for HHFW power on NSTX is to provide bulk electron heating during the I_p flat top when the plasma is heated by NBI and in H-mode. Improved HHFW coupling to NBI-generated H-modes at higher I_p (0.65-0.9 MA), after extensive plasma and antenna conditioning [7], has resulted in a broad increase in $T_e(R)$ when HHFW heating is applied. Figure 4 shows results for a pair of I_p = 900 kA, $B_T(0)$ = 5.5 kG NBI, ELM-free, H-mode plasmas with 2 MW of NBI heating, one with 1.9 MW of k_ϕ = -13 m^{-1} RF power (shot 134909) and the other with only NBI heating (shot 134910). $T_e(R)$ and $n_e(R)$ at the start of RF heating (0.248 s) are almost identical. During the HHFW pulse $T_e(0)$ increases much faster in shot 134909 than 134910, while n_eL increases at about the same rate for both shots (Fig. 4(a)). At 0.340 s $n_e(R)$ is almost identical for the two shots (Fig. 4(b)) but $T_e(R)$ shows a broad increase in shot 134909 compared to shot 134910 (Fig. 4(c)). A TRANSP-TORIC analysis predicts that about 1 MW of the 1.9 MW launched from the HHFW antenna is damped inside the LCFS [8]. Of the power coupled inside the LCFS, GENRAY predicts that 75% is absorbed directly by electrons and 25% accelerates NBI fast-ions. Figure 4(d) shows the RF deposition profile at 0.340 s is very broad for both the electrons and ions, with very little RF power reaching the axis, so that I_{RFCD} is minimal in this case.

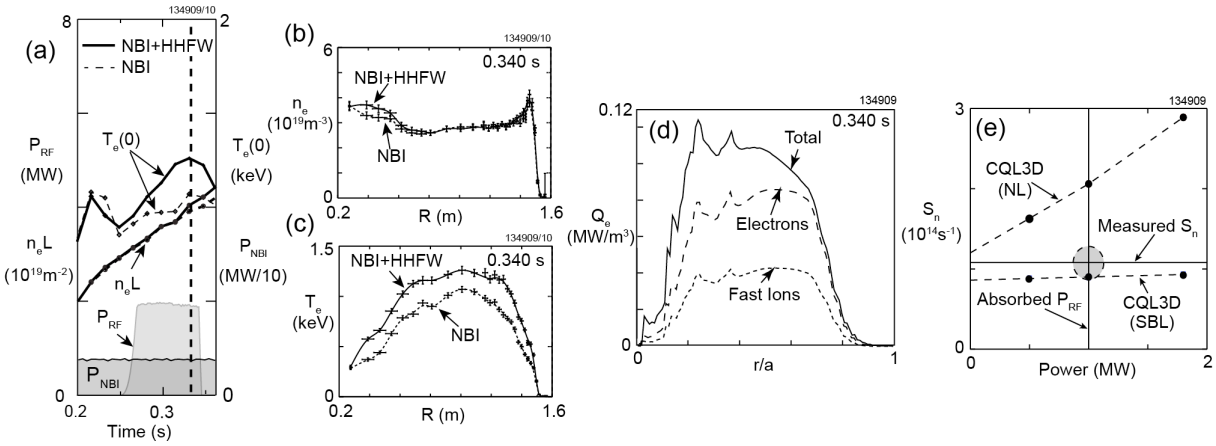

Fig. 4. (a) Time evolution of n_eL and $T_e(0)$ for two I_p = 900 kA, $B_T(0)$ = 5.5 kG H-mode plasmas with 2 MW of NBI power. One with 1.9 MW of k_ϕ= 13 m^{-1} HHFW heating (shot 134909, solid line) and the other with only NBI heating (shot 134910, dashed line). Comparison of (b) $n_e(R)$ and (c) $T_e(R)$ at 0.340s (the time indicated by the vertical dashed line in (a)). (d) RF power deposition profile versus r/a for P_{RF} = 1 MW, calculated by GENRAY for shot 134909 at 0.340 s. (e) The neutron production (S_n) predicted by CQL3D versus coupled RF power using the no loss (NL) and simple banana loss (SBL) calculation in CQL3D. The shaded circle indicates the experimental error in the measured S_n and the absorbed P_{RF}.

The CQL3D Fokker-Planck code [9] was used to compute the effect of the HHFW wave-field acceleration on the NBI fast-ions and the neutron production rate (S_n) in shot 134909. CQL3D currently provides a calculation with no fast ion loss (NL) and a simple-banana-loss calculation (SBL), which assumes trapped ions with a banana width plus Larmor radius greater than the distance to the LCFS are lost in one ion bounce time. CQL3D was run to equilibrium using kinetic profiles and equilibrium data from TRANSP for shot 134909 at 0.340 s. The results are summarized in Fig. 4(e). For P_{RF} = 1 MW, the absorbed power predicted by the TRANSP-TORIC analysis, the NL calculation predicts $S_n = 2.06 \times 10^{14}\ s^{-1}$, much higher than the measured S_n of $1.1 \pm 0.2 \times 10^{14}\ s^{-1}$, while the SBL calculation predicts $S_n = 0.9 \times 10^{14}\ s^{-1}$. These results are consistent with 60% of the RF power to fast-ions being promptly lost.

The authors wish to acknowledge the support of Drs. Masayuki Ono and Jonathan Menard, the NSTX team and the machine, RF, and neutral beam operations groups. Funding for this research was provided under USDOE Contract No. DE-AC02-09CH11466 and DE-AC05-00OR22725.

References

[1] C. E. Kessel, *et al*., Nucl. Fusion **45**, 814 (2005).
[2] P. M. Ryan, *et al*., 19th IAEA Fusion Energy Conf. Lyon, France (2002) paper EX/P2-13.
[3] R. Raman, *et al*., Nucl. Fusion **47**, 792 (2007).
[4] A. P. Smirnov, *et al*., Proc. 15th Workshop on ECE and ECRH, World Scientific (2009), pp. 301-306.
[5] M. Brambilla, *Plasma Phys. Control. Fusion* **44**, 2423 (2002).
[6] R. J. Hawryluk, in *Physics of Plasmas Close to Thermonuclear Conditions*, *Proc. of the International School of Plasma Physics*, (Pergamon, Varenna, Italy, 1981), Vol. 1, p. 1
[7] G. Taylor, *et al*., *Phys. Plasmas* **17**, 056114 (2010).
[8] B. P. LeBlanc, *et al*., 23rd IAEA Fusion Energy Conf., Daejon, Korea (2010) paper EXW/P7-12.
[9] R. W. Harvey and M. G. McCoy, Proc. of the IAEA TCM on Advances in Simulation and Modeling of Thermonuclear Plasmas, (1992).